ADVANCED FUNCTIONAL MATERIALS
www.afm-journal.de

Using Molecular Design to Increase Hole Transport: Backbone Fluorination in the Benchmark Material Poly(2,5-bis(3-alkylthiophen-2-yl)thieno[3,2-*b*]-thiophene (pBTTT)

*Pierre Boufflet, Yang Han, Zhuping Fei, Neil D. Treat, Ruipeng Li, Detlef-M. Smilgies, Natalie Stingelin, Thomas D. Anthopoulos, and Martin Heeney**

The synthesis of a novel 3,3′-difluoro-4,4′-dihexadecyl-2,2′-bithiophene monomer and its copolymerization with thieno[3,2-*b*]thiophene to afford the fluorinated analogue of the well-known poly(2,5-bis(3-alkylthiophen-2-yl) thieno[3,2-*b*]-thiophene) (PBTTT) polymer is reported. Fluorination is found to have a significant influence on the physical properties of the polymer, enhancing aggregation in solution and increasing melting point by over 100 °C compared to nonfluorinated polymer. On the basis of DFT calculations these observations are attributed to inter and intramolecular S···F interactions. As a consequence, the fluorinated polymer PFBTTT exhibits a fourfold increase in charge carrier mobility compared to the nonfluorinated polymer and excellent ambient stability for a nonencapsulated transistor device.

1. Introduction

Polythiophenes and thiophene containing derivatives have been the subject of much research in the field of organic semiconductors, owing to their relative stability, ease of synthesis, tuneable energy levels, and propensity for self-assembly. The popularity of poly(3-hexylthiophene) (**P3HT**) as an active material in both organic-field-effect transistors (OFETs) and organic photovoltaics has led to many derivatives being investigated over the past decade.[1–3] In many semicrystalline polymers such as polythiophene derivatives, increased aggregation strongly correlates with increased transistor performance, providing the polymer aggregates and crystallites are appropriately interconnected with so-called 'tie-molecules'.[4–7] Processing techniques such as thermal and solvent-vapor annealing, solvent choice for casting, and film-forming methods all affect the degree of aggregation and therefore device performance.[8–10] Rational design of the monomer repeat unit is also a useful tool to manipulate the aggregation behavior, and approaches have included fusing of aromatic rings, alterations in the alkyl chain density and regiochemistry, and heteroatom modification.[11,12]

One of the most successful and widely studied polythiophene derivatives is poly(2,5-bis(3-alkylthiophen-2-yl)-thieno[3,2-*b*]-thiophene) (**PBTTT**).[13] Unlike **P3HT**, **PBTTT** is a liquid crystalline (LC) polymer, and annealing in the LC phase has been shown to lead to improved charge carrier mobilities ranging from 0.1 to 1 $cm^2\ V^{-1}\ s^{-1}$.[14] **PBTTT** is comprised of a tail-to-tail alkylated bithiophene moiety copolymerized with a thieno[3,2-*b*]thiophene unit which, as well as rigidifying the backbone and increasing the ionization potential (IP), acts as a spacer between the solubilizing alkyl chains, thus allowing side-chain interdigitation.[12,15,16] Thiophene–thiophene links provide considerable flexibility to the backbone, assisting with the solubility and allowing a relatively low density of electronically insulating alkyl chains in the thin film. However, torsional disorder between adjacent thiophene monomers in the solid state can reduce backbone planarity and therefore detrimentally decrease conjugation length.[17] Such torsional disorder is due to steric interactions between linked

P. Boufflet, Dr. Z. Fei, Prof. M. Heeney
Department of Chemistry
Imperial College London
London, SW7 2AZ, UK
E-mail: m.heeney@imperial.ac.uk
Dr. Y. Han, Prof. T. D. Anthopoulos
Department of Physics
Imperial College London
London, SW7 2AZ, UK
Dr. N. D. Treat, Prof. N. Stingelin
Department of Materials
Imperial College London
London, SW7 2AZ, UK

DOI: 10.1002/adfm.201502826

P. Boufflet, Dr. Y. Han, Dr. Z. Fei, Dr. N. D. Treat, Prof. N. Stingelin, Prof. T. D. Anthopoulos, Prof. M. Heeney
Centre for Plastic Electronics
Imperial College London
London, SW7 2AZ, UK
Dr. R. Li, Dr. D.-M. Smilgies
Cornell High Energy Synchrotron Source
Wilson Laboratory
Cornell University
Ithaca, NY 14853, USA

aromatics and can be overcome by chemically fusing the units together.[12,18] Another approach is to promote nonbonding interactions between adjacent aromatic monomers to assist backbone planarization.[19–22] We were particularly interested to investigate the effect of thiophene fluorination in **PBTTT** because nonbonding S···F interactions have previously been shown to have a planarization effect in conjugated polymers.[23–27] In addition, fluorination could increase the IP of **PBTTT** as it does for **F-P3ATs**, and hence the oxidative stability of a polymer often considered as on the cusp of air stability.[13,24,25,28–30] In considering **PBTTT**, there are two possible sites of fluorination: on the fused thieno[3,2-*b*]thiophene or on the alkylated bithiophene co-monomer. We chose to explore the influence of fluorination on the bithiophene monomer because in this arrangement the fluorine substituents are 'head-to-head' with respect to each other which should maximize any possible S···F interactions.

In this manuscript, we present a comparative study of hexadecyl derivatives of **PBTTT** and poly(2,5-bis(4-fluoro-3-hexadecyl-thiophen-2-yl)thieno[3,2-*b*]-thiophene) (**PFBTTT**). We explore the effect of fluorination on backbone planarity though density functional theory (DFT), present the synthesis and characterization of these polymers, and probe the influence of fluorination on OFET performance and air stability, as well as thin film morphology through X-ray diffraction analysis and atomic force microscopy (AFM).

2. Results and Discussion

2.1. DFT Calculations

DFT calculations are a useful tool to predict and assess the potential planarity of conjugated polymers.[19] Trimeric units (for A–B copolymer systems) are often used as analogues to the polymer as they strike an appropriate balance between predicting the basic properties of interest, while allowing these calculations to be completed within reasonable computational time. For this reason, we opted to run the geometry optimization calculations on units where the hexadecyl side chains were replaced with propyl groups in order to emulate the steric bulk near the polymer backbone while keeping computational time low. The minimum energy conformations of the monomeric species were optimized using the B3LYP functional and a 6.31g(d) basis-set, and from these optimized geometries the minimum energy conformations of the corresponding trimers (**BTTT** and **FBTTT**) were calculated using the same level of theory.

The optimized ground-state geometries of the fluorinated and nonfluorinated trimers are shown in **Figure 1**a. The bithiophene link exhibits a dihedral angle (θ_1) of 12.7° in the nonfluorinated trimer, but upon fluorination this angle becomes 0.1°, indicating that the two fluorinated thiophenes are essentially coplanar. We believe this planarization is Coulombic in nature, as is the case in the aforementioned **F-P3AT** systems.[24] Mulliken charges show that both the hydrogen atom in the 4-position of the thiophene unit and the proximate sulfur atom in the neighboring thiophene ring have a slight positive charge in the **BTTT** trimer, tending to electrostatic repulsion and therefore a nonnegligible torsional angle. In contrast, in **FBTTT** the 4-position is occupied by a fluorine atom that exhibits a slight negative charge, leading to an attractive interaction, consequently reducing the torsional angle to near planarity. While we acknowledge that Mulliken charges must be treated with caution in conjugated systems, they nevertheless provide an indication of the sign of the charge on atoms, which in this case proves crucial to rationalizing the seemingly contradicting planarization incurred by substituting a hydrogen atom for a fluorine atom that has a larger covalent radius. Also of interest is the very slight planarization of the thiophene–thienothiophene link (θ_2), from 41.8° to 39.1° upon fluorination of the bithiophene unit.

The planarizing effect of the fluorine substitution is particularly evident when observing the change in potential energy as a function of θ_1 for the trimers, as shown in Figure 1b. We note that the slight asymmetry in the potential energy scan is present regardless of the rotation direction calculated. Aside from the minimum energy conformation being closer to planarity in **FBTTT**, the barrier to rotation is also much larger in **FBTTT** than **BTTT**, and the *syn* conformation of the thiophene–thiophene link is strongly disfavored in the former case. This conformation places both the fluorine atoms in close proximity, with the steric and electrostatic repulsion leading to the observed higher potential energy. This is less apparent in **BTTT**, presumably due to the smaller Van der Waals radius of hydrogen compared to fluorine, and lower partial charge (+0.15 and −0.28 respectively). A Boltzmann analysis of the relative populations at room temperature (Figure 1c) clearly illustrates this. Indeed, while **BTTT** shows a non-negligible population of *syn* thiophene–thiophene links ($\theta_1 = \pm 180°$), **FBTTT** exhibits a narrow distribution of conformations around the *trans* coplanar conformer ($\theta_1 = 0°$) and a very small proportion of the competing *syn* analogue. Together these results suggest that fluorination will result in a significant increase in the rigidity of the backbone and a preference for the *trans* coplanar conformation.

Visual representations of the HOMO and LUMO of **BTTT** and **FBTTT** trimers are shown in Figure S1 (Supporting Information). Both show extended delocalization of the two frontier molecular orbitals, typical of all-donor conjugated units.[17,44] The substitution of hydrogen atoms by fluorine in the bithiophene unit seems to have only a minimal effect on the orbital distribution, in the form of a minor contribution to both the HOMO and the LUMO.

2.2. Synthesis

Building upon our recent synthesis of short chain 3-alkyl-4-fluorothiophene derivatives, we decided to utilize the fluorinated building block **1** and introduce the hexadecyl side chain via a cross-coupling methodology (**Scheme 1**).[24] Since backbone fluorination can result in a reduction in polymer solubility, the hexadecyl side chain was chosen as it is the longest solubilizing group which has been demonstrated to still afford good FET performance in **PBTTT**.[24,28,31] Alkylation of **1** was best achieved via Negishi coupling using commercially available hexadecylzinc bromide in the presence of catalytic Pd(dppf)Cl_2. Superheating of the tetrahydrofuran (THF) solvent to 100 °C in a microwave reactor was required to afford good yields of **2**. This was purified either by reverse-phase chromatography on C18-functionalized silica using a mixed acetonitrile/THF

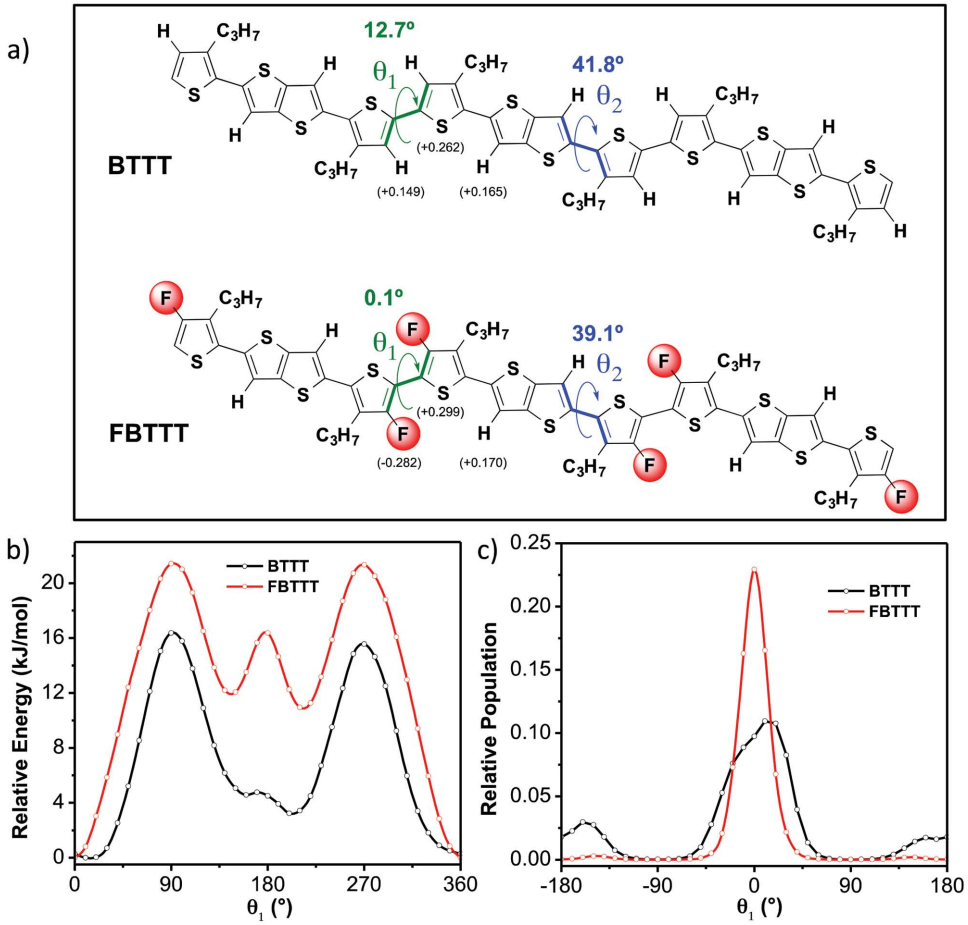

Figure 1. a) Minimum energy conformations of **BTTT** and **FBTTT** trimer units with key dihedral angles highlighted (θ_1 and θ_2). Mulliken charges on key atoms are indicated in parentheses. b) Potential energy scan of the **BTTT** and **FBTTT** trimers as a function of θ_1. c) Relative Boltzmann population of conformations at 298 K as a function of rotation from *trans*-coplanar ($\theta_1 = 0°$).

eluent, or the crude mixture was deprotected to give **3**, which was then purified by normal-phase flash chromatography on silica. We opted for the latter for larger scale reactions, since unfunctionalized silica can support a higher loading capacity.

Tail-to-tail dimerization of 3-alkylthiophenes is usually easily achieved through lithiation followed by oxidative coupling using copper(II) chloride.[32] Though the initial lithiation of **3** was achieved, as confirmed by quenching with a solution of iodine in dry THF, the oxidative coupling step proved problematic. Evidently, the fluorine substitution at the 4-position plays a role in hindering the oxidative coupling with copper(II) chloride. We therefore decided to regioselectively metallate **3** using the sterically hindered Knochel–Hauser base before adding 0.5 equivalents of $Ni(dppp)Cl_2$. Reductive elimination from the resulting Ni(II) salt afforded the desired tail-to-tail bithiophene **4** in good yield (73%). Subsequent bromination led to monomer

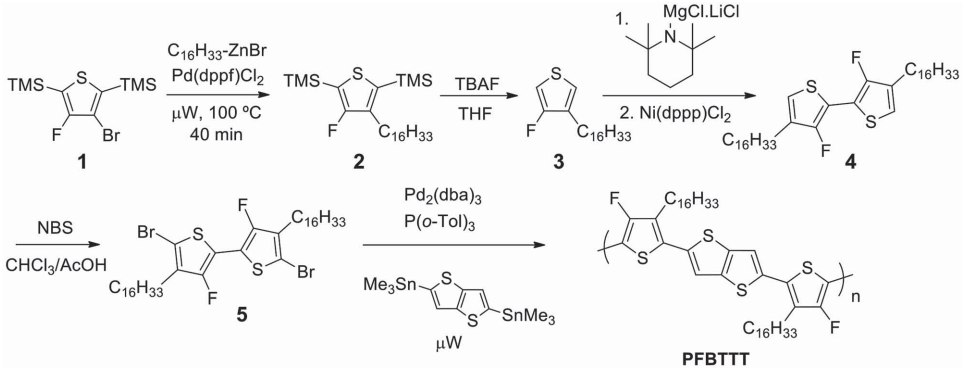

Scheme 1. Synthesis of the fluorinated bithiophene monomer **4** and **PFBTTT** via microwave-assisted Stille polycondensation reaction.

5, which was copolymerized with 2,5-bis(trimethylstannyl) thieno[3,2-*b*]thiophene under microwave polymerization conditions to yield **PFBTTT**.[33] For comparison purposes, **PBTTT** was synthesized under identical microwave polymerization conditions. Both polymers were purified by precipitation and subsequent Soxhlet extraction with methanol, acetone, and hexane to remove catalyst impurities and low molecular weight oligomers. In the case of **PFBTTT** the crude polymer was also extracted with chloroform to remove low molecular weight polymeric material, before extraction into chlorobenzene. In both cases, a final purification by precipitation of chlorobenzene solutions into methanol was performed.

2.3. Physical Properties

In order to ensure a fair comparison and exclude molecular weight effects, which are known to affect the performance of **PBTTT**,[34–36] we compared batches of similar molecular weight distribution **PBTTT** and **PFBTTT** (M_n 42 kDa, $Đ$ 1.5 and M_n 44 kDa, $Đ$ 2.0, respectively, as measured by high-temperature gel-permeation chromatography (HT GPC) against polystyrene standards). The basic physical properties of **PFBTTT** all tend to suggest a greater degree of aggregation when compared to its nonfluorinated analogue **PBTTT**. First, **PFBTTT** is only soluble in near-boiling chlorobenzene, rendering processing from this traditional solvent difficult. We therefore adopted 1,2,4-trichlorobenzene (TCB) as a solvent for most processing techniques due to its good solubilizing properties and high boiling point. In TCB, **PFBTTT** is readily soluble at temperatures exceeding 135 °C, yet precipitates soon after cooling to 130 °C, while **PBTTT** remains soluble for several minutes at room temperature.

The solution UV–vis spectra of **PBTTT**, both hot and at room temperature, exhibit a single broad absorption band typical of fully solvated polythiophene derivatives (**Figure 2** and **Table 1**).[37] The slight blueshift of 12 nm of the absorption maximum upon increasing the solution temperature is attributed to the increased backbone torsion, which reduces the effective conjugation length. In contrast, the hot and room temperature solution spectra of **PFBTTT** are very different. The hot solution spectrum shows that the majority of the absorption arises from solvated polymer, similar to **PBTTT**. There is very little difference in λ_{max} for the two polymers in hot solution. When the **FBTTT** solution is cooled, the absorption spectrum redshifts by 69 nm to give an absorption spectrum which strongly resembles that of the thin film, suggesting the polymer has planarized and aggregated in solution, similar to the formation of polythiophene aggregates in poor solvents.[38–41] Even in the hot solution, the presence of a slight shoulder at higher wavelengths suggests some aggregate is still present.

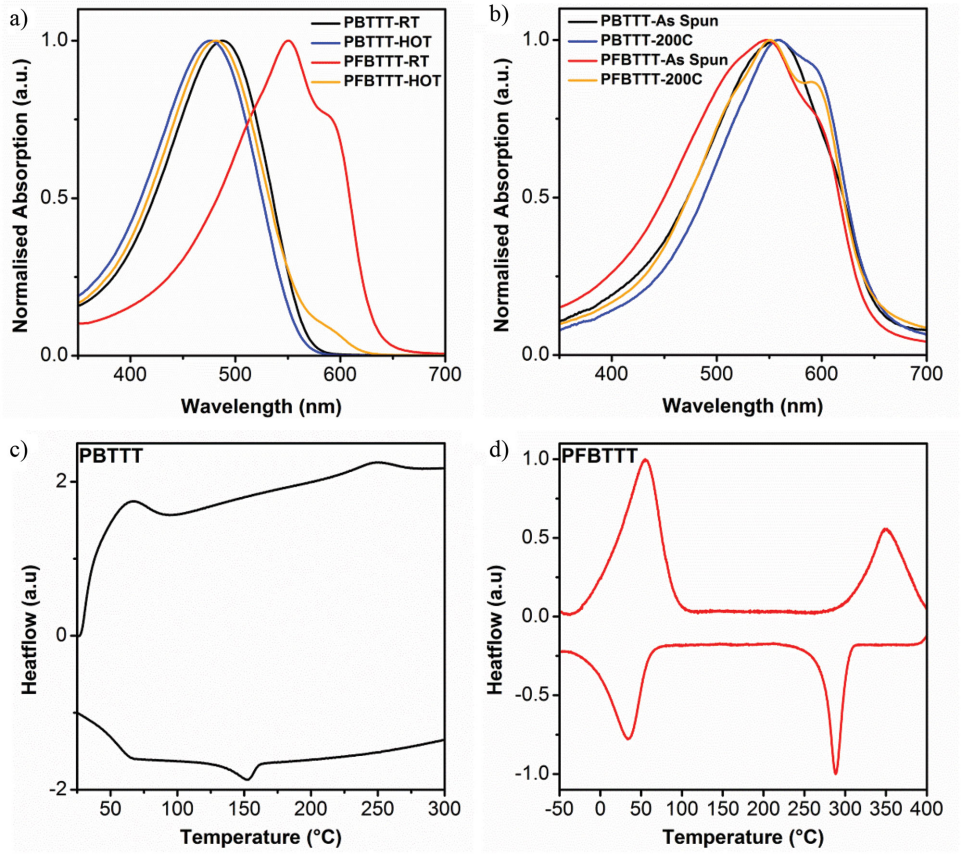

Figure 2. a) Solution UV–vis spectra of **PBTTT** and **PFBTTT** in TCB at room temperature (RT) and hot solutions (>80 °C). b) UV–vis spectra of as spun and annealed (200 °C) thin films of **PBTTT** and **PFBTTT**. c,d) Flash DSC traces of **PBTTT** and **PFBTTT**, respectively (heating and cooling rate of 500 K s^{-1}).

Table 1. Summary of physical properties of **PBTTT** and **PFBTTT**.

		λ_{max} [nm]					DSC transition temperatures [°C][g]	
Polymer	M_n [kDa $Đ^{-1}$][a]	Solution (hot)[b]	Thin film[c]	E_g, opt [eV][d]	IP [eV][e]	LUMO [eV][f]	T_{m1}/T_{m2}	T_{c1}/T_{c2}
PBTTT	42.1/1.5	488 (476)	559 (591)	1.91	–5.10	3.19	67/249	55/151
PFBTTT	44.2/2.0	550 (481)	547 (510, 594)	1.93	–5.10	3.17	65/353	33/288

[a]Measured in 1,2,4-trichlorobenzene (TCB) at 140 °C relative to polystyrene standards; [b]Measured in room temperature TCB, or hot (>80 °C) TCB in parentheses; [c]Films spin-coated from TCB; [d]Optical band gap estimated from the absorption onset of as-spun films; [e]Ionization potential measured by photoelectron spectroscopy in air (PESA) error ± 0.05 eV; [f]Lowest unoccupied molecular orbital estimated from the optical band gap and PESA measurements; [g]Measured by flash DSC at heating and cooling rates of 500 K s^{-1}.

Upon thin film formation, both polymers display a redshift in λ_{max} of around 70 nm compared to the hot solutions as the polymers planarize in the solid state. In the case of **PFBTTT**, this is accompanied by the appearance of pronounced shoulders both at longer and shorter wavelengths. These shoulders are typical of the vibronic progression observed in many polythiophenes and ascribed to the formation of ordered aggregates in the film. For **PBTTT**, the vibronic features are less obvious in the as-spun film, but become sharper upon thermal annealing at 200 °C. Thermal annealing also results in changes to the **PFBTTT** spectra, with the longer wavelength shoulder increasing in intensity and the short wavelength diminishing. These changes are consistent with some structural reordering in the films upon annealing. Both polymers exhibit very similar optical band gaps, as measured by the absorption edge of the as-spun films (Table 1). Thermal annealing results in films with an identical band gap.

The effect of the fluorination on the IP of thin films was minimal, with no difference observed within the experimental error (±0.05 eV) of the measurement by photoelectron spectroscopy in air (PESA) (Table 1). This is in contrast to the results for **F-P3AT**s, in which a clear (≈0.25–0.4 eV) increase in IP was observed in comparison to the analogous **P3AT**s, as well as a widening in the optical band gap.[24] The DFT calculations suggest that fluorination would result in a modest stabilization of the HOMO of 0.16 eV and the LUMO of 0.18 eV over the nonfluorinated trimer. The difference between the experimental and the theoretical results may therefore be related to error of the PESA measurement, since we note that the transistor results (vide infra) show higher contact resistance for the fluorinated polymer over the nonfluorinated polymer, which would support a slight increase in IP upon fluorination.

The thermal properties of the two polymers were investigated by differential scanning calorimetry (DSC). Our initial experiments utilized conventional DSC at heating rates of 10°C min^{-1} (Figure S13, Supporting Information). In these experiments, we were able to clearly observe the LC phase of **PBTTT**, with two well-defined endotherms on heating, at 126 and 238 °C, which have previously been attributed to a side chain and backbone melt.[42,43] However, despite heating to 390 °C, we could not observe a well-defined backbone melt for **PFBTTT**. We therefore moved to flash DSC in which heating rates of 500 K s^{-1} are obtainable. Such rapid heating and cooling rates increase the sensitivity of the measurement and also allow the investigation of temperatures regimes not readily accessible with conventional DSC due to competing decomposition processes. The flash DSC thermograms of both polymers are shown in Figure 2. The effect of the two fluorine atoms on the thermal properties is remarkable, with an increase in the backbone melt of approximately 100°C, from 250°C for **PBTTT** to 350 °C for **PFBTTT**. Note that melting enthalpies are not readily accessible with flash DSC due to the small sample size. This increase is much more substantial than would be expected by a simple molecular weight argument (based upon the increased atomic mass of F over H), and is therefore supportive of the increased intra- and intermolecular interactions that would result from the more coplanar bithiophene unit suggested by DFT calculations. It is also interesting that the temperature of the low-temperature endotherm reduces upon fluorination, from 66 to 55 °C. A similar reduction in side-chain melting point is observed for a **PBTTT** analogue in which the alkyl side chains are moved from the bithiophene unit, in which each thiophene can rotate independently, to a thieno[3,2-b]thiophene in which case each alkyl side chain must move co-operatively.[30] A similar co-operative movement of the side chains might be expected for the fluorinated bithiophene if the S...F interaction was pronounced, as suggested by the DFT calculations. Finally, we note that thermogravimetric analysis of **PFBTTT** demonstrates that it exhibits excellent thermal stability, with 5% weight loss occurring only beyond 420 °C (Figure S14, Supporting Information).

2.4. Transistor Fabrication and Characterization

The electrical properties of the polymers were studied employing thin film transistors. Films were prepared by spin-coating from TCB in both cases, followed by annealing at 200 °C for 30 min. We note that the transistor performance of **PBTTT**, to the best of our knowledge, has not been previously reported for films cast from TCB. Bottom-gate top-contact configuration devices for both polymers exhibit typical unipolar hole transporting behavior with low hysteresis between the forward and reverse gate voltage (V_G) sweeps and moderate on/off channel current ratios of ≈10^3–10^4, as shown in **Figure 3**. It is notable that both the peak and average charge carrier mobility values increase upon fluorination by approximately a factor of 4, with the best devices exhibiting a saturated mobility of ≈0.32 cm^2 V^{-1} s^{-1} for the fluorinated polymer, compared to ≈0.069 cm^2 V^{-1} s^{-1} for the nonfluorinated analogue. The performance data of the two polymers is summarized in **Table 2**. Although significantly lower than the record charge carrier mobilities recorded for

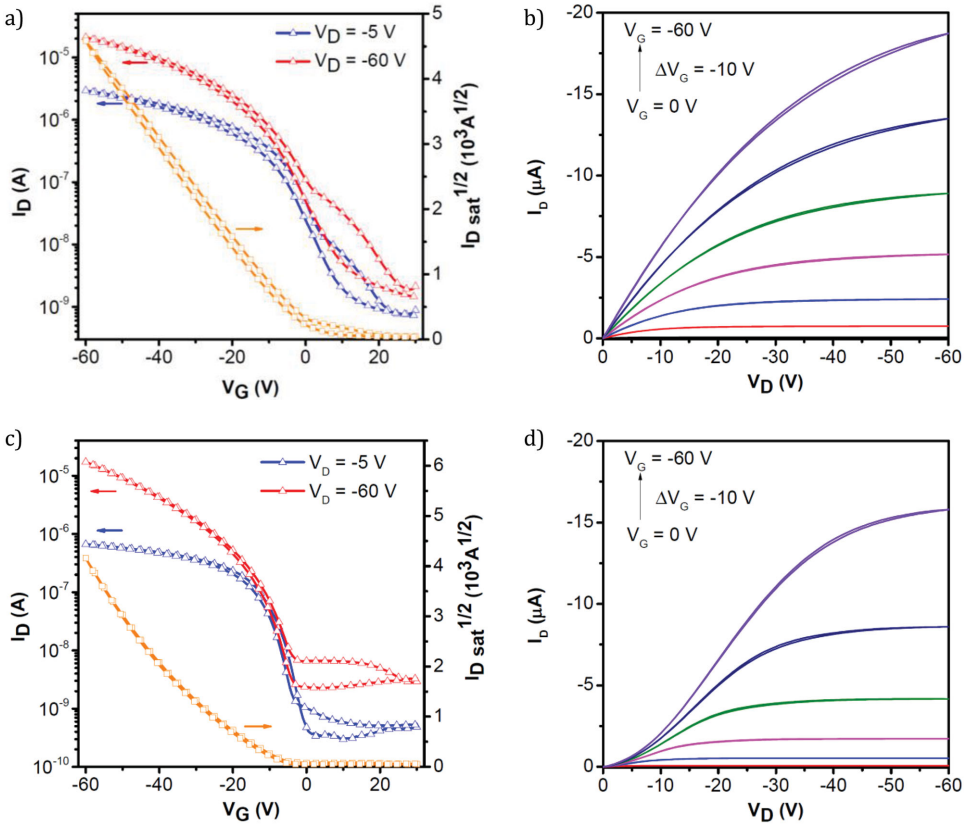

Figure 3. a,c) Transfer characteristics of **PBTTT** and **PFBTTT**, respectively. b,d) Output characteristics of **PBTTT** and **PFBTTT**, respectively. Devices made in bottom-gate top-contact configuration, with channel width and length of 1000 and 50 μm, respectively.

donor–acceptor polymers, these values are still high for an all-donor system.[17,44] While the mobilities reported here for **PBTTT** devices (max 0.069 $cm^2\ V^{-1}\ s^{-1}$) are lower than those often reported in the literature (0.1–1 $cm^2\ V^{-1}\ s^{-1}$), we attribute this mainly to the longer hexadecyl alkyl-chain length used in our case (as opposed to tetradecyl used previously in higher performing **PBTTT**-based transistors), as well as the different processing solvent (TCB compared to mixtures of chloroform and chlorobenzene). In fact, the few reports of hexadecyl-substituted **PBTTT** transistor properties involve either highly optimized and rigorous device fabrication process or a tailored 'spread-and-compress' film formation on top of an ionic liquid.[29,45,46] The marginally higher threshold voltages (V_{TH}) required for **PFBTTT** devices along with the slightly sigmoidal output curves and the increasing slope of the $I_{sd}^{1/2}$ versus V_g curve suggest increased contact resistance and/or localized high-energy trap states for **PFBTTT** over **PBTTT**.[47] Previously, the use of high work function electrodes like Pt has been shown to reduced contact resistance in **PBTTT** and may provide a possible solution to further improve device performance.[14]

Table 2. Summary of OFET performance of devices in bottom-gate top-contact configuration.

Polymer	μ [$cm^2\ V^{-1}\ s^{-1}$]		V_{th} [V]	V_{on}/V_{off}
	Linear	Saturated (peak value)		
PBTTT	0.048 ± 0.013	0.058 ± 0.0086 (0.069)	−0.3 ± 0.6	10^3–10^4
PFBTTT	0.13 ± 0.067	0.23 ± 0.07 (0.32)	−17.8 ± 3.0	10^3–10^4

Previous reports have demonstrated that fluorination of the conjugated side chain or backbone can result in improved device stability in the presence of ambient air, with the effect being ascribed to either an increase in the IP as a result of the electron withdrawing influence of fluorine or to a kinetic effect reducing water ingress due to closer packing of the conjugated molecules in the solid state.[48,49] Therefore, we investigated the stability of the **PBTTT** and **PFBTTT** devices by removing them from the glove box and storing them in the dark under ambient conditions with an average temperature of 20 °C and relative humidity of 50%. The air-stability of **PBTTT**-based devices varies considerably in the literature. In the case of C_{12}- and C_{14}-**PBTTT** devices, stability in ambient conditions is known to be quite poor, with off current rising and charge mobility dropping to about 20% of the original value after 5 and 22 d, respectively.[13,30] Humidity was shown to have a significant deleterious impact on the charge carrier mobility, with storage at low humidity shown to drastically improve the operational lifetime of these devices.[30] High humidity levels have been shown to result in the formation of charge traps in the film in studies on related polythiophenes.[50] It is worth noting that the increase in off-current and shift in threshold voltage reported for many polythiophene derivatives may not be due solely to the effects of oxygen or water, but also to minor impurities in ambient air such as ozone, which can act as a reversible dopant

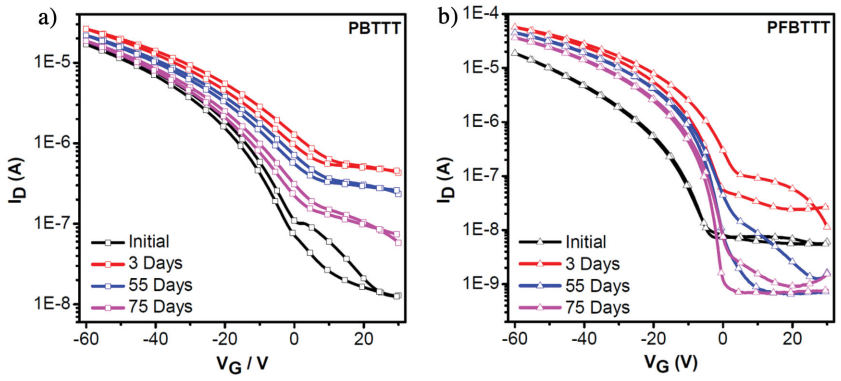

Figure 4. Stability study of a) **PBTTT** and b) **PFBTTT** devices stored in ambient conditions (20 °C and 50% relative humidity).

for the polymer.[51] To our knowledge, the only stability study performed on the C_{16}-**PBTTT** was performed by Umeda et al. in which repeated stressing in ambient conditions over 2 d had little impact on the field effect characteristics such as mobility and on/off ratio.[29]

The transfer plots of **PBTTT** and **PFBTTT** after 3, 55, and 75 d storage in the dark in ambient air are shown in **Figure 4** and the data are summarized in **Table 3**. For both polymers the charge carrier mobility remained relatively constant over the test period, but we did observe changes in the threshold voltage and on/off channel current ratio over time. In particular, the off current rose rapidly after 3 d, with a large positive shift in the threshold voltage for both materials. Upon continued storage the threshold voltage moved back toward the original values, and the off currents dropped. The fluorinated polymer consistently maintained a higher on/off ratio than **PBTTT**, with the device after 75 d exhibiting a value around 5×10^4. The **PFBTTT** transistor also demonstrated a sharper turn-on with a narrower subthreshold swing than **PBTTT**. As discussed above, the shifts in threshold and increase in off-current are typical of oxidative doping making the device more conductive, and as such difficult to switch-off. The fluctuations in threshold and off ratio over time suggest that this doping is reversible, and the lower currents for the fluorinated polymer suggest it is less susceptible to such doping, in common with other fluorinated materials.[22,52]

2.5. Thin Film Morphology

While it is widely accepted that **PBTTT** possesses a high degree of order in the lamellar direction, the π-stacking direction exhibits a relatively high degree of paracrystallinity.[53,54] The factors that allow **PBTTT** to have high hole mobilities are therefore considered to be its relatively low-energy trap states and high edge-on orientation.[53–55] In order to assess the impact of **PBTTT** fluorination on its orientational order, we performed grazing incidence wide-angle X-ray scattering (GIWAXS) on films prepared in the same way as the OFET devices (**Figure 5**). Both films exhibit diffraction patterns consistent with lamellar ordering of the polymers with an edge-on orientation with respect to the substrate. In the as cast films, the crystalline domains of **PFBTTT** possesses a higher degree of edge-on orientation, which is apparent from the more localized out-of-plane scattering patterns corresponding to diffraction in the lamellar direction. Indeed, arcing of these diffraction peaks is attributed to misalignment of the crystallites with respect to the surface.[15] The lamellar spacing is similar for both polymers, at 2.33 nm for **PFBTTT** and 2.35 nm for **PBTTT**. This is in agreement with the *d*-spacing previously observed for C_{16}-**PBTTT** and suggests that the alkyl side chains of adjacent polymer backbones are interdigitated for both polymers.[56] Annealing the films results in an increase in the intensity of the diffraction peaks for both polymers, most clearly observed in the out-of-plane line profiles in the Supporting Information (Figure S15). The *d*-spacing does not change for **PFBTTT**, while it slightly narrows for **PBTTT** to 2.315 nm, suggesting either enhanced crystallinity or a change in crystal orientation in the film. That the in-plane lamellar diffraction peaks gradually disappear for **PFBTTT** with annealing would suggest the latter, that the misaligned polymer domains reorientate to become predominately edge-on. For **PBTTT**, the out-of-plane peaks also increase in intensity and the arcing reduces, consistent with a similar increase in edge-on alignment. However the in-plane scan suggests that the misaligned domains remain upon annealing (Figure S15, Supporting Information), which was not the case for **PFBTTT**. High-resolution X-ray diffraction measurements also show an increase in intensity of the (100) and corresponding higher order diffraction peaks upon annealing for both polymers (Figure S16, Supporting Information), thus confirming the increased crystallinity suggested by GIWAXS. The greater orientational order in **PFBTTT** compared to **PBTTT** could therefore be one of the factors resulting in the increase in mobility upon fluorination. We also note that **PBTTT** films annealed at 150 °C exhibit a split in the (100) and higher order out-of-plane signals, possibly due to different degrees of interdigitation, and side-chain reorganization.

The surface morphology of the films was also investigated by AFM in films made under the same conditions as used for device fabrication. The first point to note is that the film morphology achieved for **PBTTT** from spin-coating from TCB

Table 3. Summary of OFET lifetime characteristics for **PBTTT** and **PFBTTT** from 0 to 75 d.

Polymer	μ_{sat} [cm^2 V^{-1} s^{-1}]				V_{TH} [V]				Channel current on/off ratio			
	0 d	3 d	55 d	75 d	0 d	3 d	55 d	75 d	0 d	3 d	55 d	75 d
PBTTT	0.058	0.059	0.058	0.059	−1	13	8	1	2.6×10^2	5.8×10^1	7.3×10^1	2.0×10^2
PFBTTT	0.18	0.20	0.17	0.16	−22	4	−3	−6	2.8×10^3	2.3×10^3	6.6×10^4	5.3×10^4

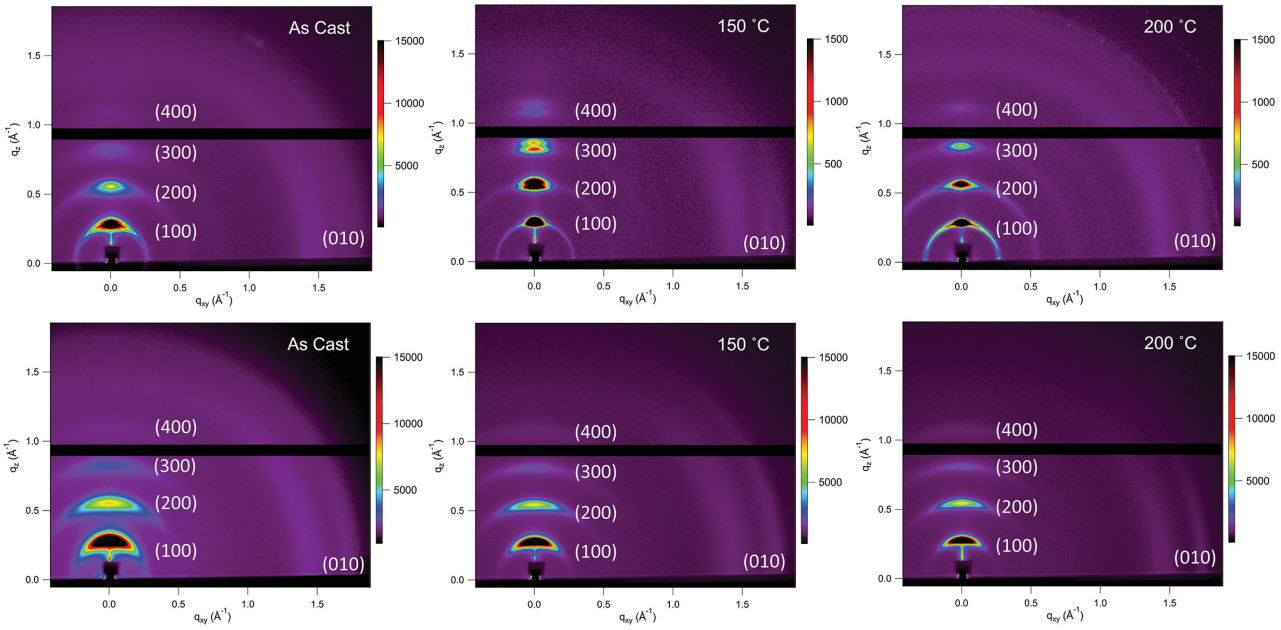

Figure 5. 2D Grazing Incidence Wide-Angle X-ray Scattering (GIWAXS) patterns of **PBTTT** (top) and **PFBTTT** (bottom) as a function of annealing temperature.

is very different from the terraced nanostructure observed when spin-coating from other solvents such as 1,2-dichlorobenzene and chloroform.[13,34,42] Indeed we observe that **PBTTT** appears to have a large quantity of pin holes distributed across the whole film (Figure S17, Supporting Information), which were likely formed by the solvent-vapor bubbles during drying. Although films of **PBTTT** and **PFBTTT** have similar a similar RMS roughness (6.79 nm and 6.99 nm respectively), these holes probably have a detrimental effect on the continuity of the film and introduce extra traps, potentially hindering the transport of charge carriers. However, in the case of **PFBTTT**, we observe a film comprised of a more fibrillar morphology (Figure S17, Supporting Information). Though highly entangled, the fibrillar structure could facilitate the release of solvent vapor, leaving a more continuous film with fewer pinholes. In fact, when diluted to 2 mg mL^{-1}, **PFBTTT** forms interconnected nanofibrils, with heights of approximately 5 nm and widths of 200–500 nm (**Figure 6**), unlike **PBTTT** under the same dilution (Figure S18, Supporting Information). This network of intricately woven fibers could be a morphological explanation for the increased mobility observed in **PFBTTT**. Indeed, recent studies have shown that interconnectivity of ordered domains is crucial to achieve high mobilities with polythiophene derivatives.[2,21,22]

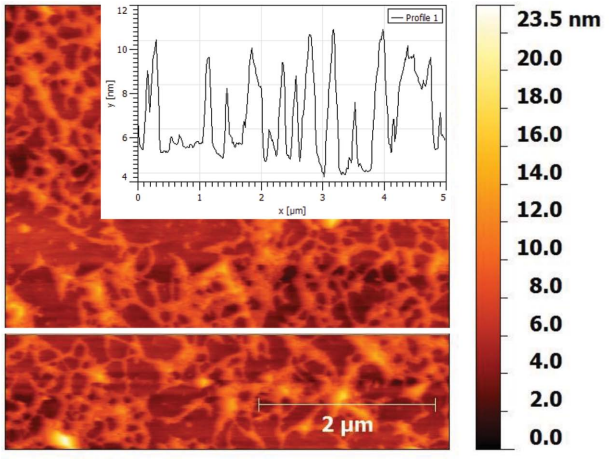

Figure 6. AFM (topography) of **PFBTTT** spin-coated from TCB at concentration of 2 mg mL^{-1}, showing interconnected fibrillar network of polymer domains. Inset topographical profile corresponds to scan along the white line.

3. Conclusions

In conclusion, we have described the synthesis of a novel 3,3′-difluoro-4,4′-dihexadecyl-2,2′-bithiophene monomer and report its copolymerization with thieno[3,2-*b*]thiophene to afford the fluorinated analog of the well-known **PBTTT** polymer. We find that backbone fluorination has a pronounced influence on the physical properties of the polymer, with a significantly enhanced degree of aggregation compared to the nonfluorinated analog. Remarkably, we find that the incorporation of just two fluorine atoms on the polymer backbone results in an increase in the polymer melting temperature of 100 °C. DFT calculations suggest this increased aggregation originates from a greater degree of backbone planarity and rigidity. A result of this greater rigidity is an enhancement of the edge-on orientational order, and consequently a significant increase in hole mobility in OFET devices, which is also aided by an appreciably interwoven fibrillar morphology. In addition, the fluorinated polymer exhibits excellent ambient stability for a nonencapsulated transistor device. We believe

that these results demonstrate that backbone fluorination is a useful tool in designing high-performance organic semiconductors.

4. Experimental Section

Materials: Reagents and chemicals were purchased from Aldrich and Acros, except hexadecylzinc bromide, which was purchased from Rieke Metals. All reactions were carried out under argon using anhydrous solvents and reagents as commercially supplied, unless otherwise stated. **PBTTT**, 2,5-bis(trimethylstannyl)thieno[3:2-*b*]thiophene and 3-bromo-4-fluoro-5-bis(trimethylsilyl)thiophene (**1**) were synthesized as previously reported.[13,24] Melting points were taken as peak maximum of DSC traces in all cases.

Synthesis of 3-Fluoro-4-Hexadecylthiophene (3): In a dry 20 mL Biotage microwave vial under argon, **1** (2.00g, 6.15 mmol), and [1,1′-bis(diphenylphosphino)ferrocene]dichloropalladium(II) dichloromethane complex (251 mg, 0.307 mmol) were added. The vial was capped, evacuated, and backfilled with argon three times, before adding hexadecylzinc bromide solution (16.0 mL, 0.5 M in THF). After stirring at room temperature for 2 min, the vial was heated for 1 h in a microwave reactor at 100 °C. The resulting mixture (solid at room temperature) was heated to 40 °C, poured into acetone, and filtered. The solvent of the filtrate was removed in vacuo, and the residue passed through a pad of silica using hexane, and the solvent was again removed in vacuo. In a 100 mL round-bottomed flask, the resulting crude mixture of **2** was dissolved in dry THF (10 mL) and cooled to 0 °C before *N*-tetrabutylammonium fluoride (21.5 mL, 1 M solution in THF) was added. The reaction was stirred for 2 h before quenching with water and extracting with diethyl ether. The organic extracts were dried over $MgSO_4$ and the solvent removed in vacuo. The crude mixture was purified by column chromatography on silica, using hexane as eluent, to yield **3** as a white waxy solid (300 mg, 15% over two steps). mp: 27 °C; ^{1}H NMR (400 MHz, $CDCl_3$, δ): 6.82 (1 H, dd, *J* 3.8 & 3.6), 6.64 (1 H, d, *J* 3.6), 2.53 (2 H, t, *J* 7.6), 1.69–1.54, (2 H, m), 1.37–1.21 (26 H, m), 0.89 (3 H, t, *J* 6.8); ^{13}C NMR (100 MHz, $CDCl_3$, δ): 156.92 (d, *J* 259.0), 131.86 (d, *J* 23.2), 119.67 (d, *J* 7.8), 102.77 (d, *J* 21.5), 31.97, 29.73, 29.70, 29.61, 29.41, 29.29, 29.26, 26.83, 22.73, 14.15; ^{19}F NMR (377 MHz, $CDCl_3$, δ): –132.25; HRMS (EI) *m/z*: $[M+H]^+$ calcd for $C_{20}H_{35}FS$, 326.2444; found, 326.2452.

Synthesis of 3,3′-Difluoro-4,4′-Dihexadecyl-2,2′-Bithiophene (4): In a dry 20 mL Biotage microwave vial under argon, **3** (400 mg, 1.23 mmol) was dissolved in dry THF (3.5 mL), and (2,2,6,6-tetramethylpiperidinyl) magnesium chloride lithium chloride complex (1.59 mL, 1 M solution in THF/toluene) was added dropwise at room temperature. The reaction was stirred for 1 h before a dispersion of [1,3-bis(diphenylphosphino)propane] dichloronickel(II) (333 mg, 0.615 mmol) in dry THF (7 mL) was added. The solution turned from orange to dark brown/black and solidified. After diluting with THF, the reaction mixture was poured into dilute HCl and extracted with chloroform. The solvent was removed in vacuo, and the residue passed through a small pad of silica using dichloromethane as eluent. The solvent was removed in vacuo, and recrystallized from acetone, to yield **4** as a pale yellow solid (290 mg, 73%). Crystals were grown from hexane for melting point analysis. mp (hexane): 92 °C; ^{1}H NMR (400 MHz, $CDCl_3$, δ): 6.80 (2 H, d, *J* 3.1), 2.52 (4 H, t, *J* 7.8), 1.67–1.56 (4 H, m), 1.37–1.21 (52 H, m), 0.88 (6 H, t, *J* 6.7); ^{13}C NMR (100 MHz, $CDCl_3$, δ): 152.46 (d, *J* 263.3), 131.86 (d, *J* 23.4), 117.97 (t, *J* 7.0), 110.0, 31.94, 29.70, 29.67, 29.57, 29.37, 29.24, 29.07, 27.01, 22.70, 14.13; ^{19}F NMR (377 MHz, $CDCl_3$, δ): –128.94 (d, *J* 3.4).

Synthesis of 5,5′-Dibromo-3,3′-Difluoro-4,4′-Dihexadecyl-2,2′-Bithiophene (5): In a 100 mL round-bottomed flask wrapped in foil, **4** (265 mg, 0.408 mmol) was dissolved in a mixture of chloroform (20 mL) and acetic acid (3 mL), and to this solution was added *N*-bromosuccinimide (154 mg, 0.815 mmol). The solution was stirred overnight, quenched with saturated sodium sulfite, and extracted with chloroform. The organic layer was washed with 1 M sodium hydroxide, water, and brine, and the solvent was removed in vacuo. The crude product was recrystallized from a mixture of acetone and ethyl acetate (1:1), to yield **5** as a pale yellow solid (245 mg, 75%). mp (hexane): 87 °C; ^{1}H NMR (400 MHz, $CDCl_3$, δ): 2.53 (4 H, d, *J* 7.4), 1.60–1.50 (4 H, m), 1.39–1.09 (52 H, m), 0.88 (6 H, t, *J* 6.8); ^{13}C NMR (100 MHz, $CDCl_3$, δ): 150.77 (d, *J* 266.8), 131.74 (d, *J* 23.9), 111.10 (d, *J* 10.7), 108.56 (d, *J* 8.7), 31.94, 29.71, 29.68, 29.64, 29.53, 29.38, 29.31, 29.14, 28.51, 26.78, 22.71, 14.13; ^{19}F NMR (377 MHz, $CDCl_3$, δ): –123.81; Anal. calcd for $C_{40}H_{66}Br_2F_2S_2$: C 59.39, H 8.22; found: C 59.53, H 8.31.

Synthesis of Poly[2,5-bis(4-fluoro-3-hexadecyl-thiophen-2-yl)thieno-[3,2-b]-thiophene] (PFBTTT): In a dry 0.5–2 mL Biotage microwave vial, **6** (202.9 mg, 0.2509 mmol), bis(2,5-trimethylstannyl)thieno[3:2-*b*] thiophene (116.9 mg, 0.2509 mmol), tris(dibenzylideneacetone) dipalladium(0) (4.1 mg, 2 mol%), and tris(*o*-tolyl)phosphine (6.1 mg, 8 mol%) were added, and the vial capped and evacuated for 10 min. After backfilling with argon, degassed chlorobenzene (1.2 mL) was added, and the solution was degassed for a further 10 min. The mixture was then heated in a microwave in steps as follows: 100, 120, 140, 160 °C for 2 min each, and finally 180 °C for 30 min. After cooling to room temperature, the dark purple gel was precipitated in methanol from chlorobenzene, and purified by Soxhlet extraction (glass thimble), washing with methanol, acetone, hexane, (each overnight), chloroform (3 h), and finally extracting the polymer with chlorobenzene. Most of the solvent was removed in vacuo, before precipitating the polymer into methanol and filtering (184 mg, 93%). M_n: 44 kDa, M_w: 87 kDa; ^{1}H NMR (400 MHz, $CDCl_3$, δ): 7.41 (1 H, br s), 2.89 (3 H, br s), 1.92–1.65 (4 H, br m), 1.57–1.31 (59 H, br m), 0.96 (6 H, t, *J* 6.7).[1]; ^{19}F NMR (377 MHz, d^2-TCE, δ) –122.33; Anal. calcd for $C_{46}H_{68}F_2S_4$: C 70.53, H 9.13; found: C 70.05, H, 8.79. (Note that ^{1}NMR integration was complicated by the low solubility and aggregation in solution, leading to broad signals.)

DFT Calculations: DFT calculations were carried out using the B3LYP hybrid functional and the 6–31g(d) basis set in the GAUSSIAN09 software package.[59] Alkyl chains were replaced with a propyl group to simplify calculations and reduce computational time. Structures were optimized, and a frequency analysis was performed. Potential energy scans were performed on the trimers using the redundant coordinate editor and scanning the indicated dihedral angle in 36 steps of 10° increments.

Characterization: ^{1}H, ^{19}F, and ^{13}C NMR spectra were recorded on a Bruker AV-400 (400 MHz), using the residual solvent resonance of chloroform-*d* or 1,1,2,2-tetrachloroethane-d^2 and are given in ppm. Microwave experiments were performed in a Biotage initiator V 2.3. Polymer molecular weight and dispersity ($Đ$) analysis was completed via GPC in TCB at 140 °C using a Polymer Laboratories PL-220 HT GPC instrument calibrated against polystyrene standards. Electrospray mass spectrometry was performed with a Thermo Electron Corporation DSQII mass spectrometer. UV–vis spectra were recorded on a UV-1800 Shimadzu UV–vis spectrometer. Flash chromatography was performed on silica gel (Merck Kieselgel 60 230–400 mesh) or on reverse phase silica (Biotage SNAP KP-C18-HS cartridges). PESA measurements were recorded with a Riken Keiki AC-2 PESA spectrometer with a power setting of 5 nW and a power number of 0.5. Samples for PESA were prepared on glass substrates by spin-coating. DSC measurements, using ≈3 mg of material, were conducted under nitrogen at scan rate of 10 °C min^{-1} with a TA DSC-Q20 instrument. Flash DSC was performed on a Mettler Toledo Flash DSC 1 at a scan rate of 500 K s^{-1}. AFM images were obtained with a Picoscan PicoSPM LE scanning probe in tapping mode. GIWAXS measurements were performed at D-line, Cornell High Energy Synchrotron Source (CHESS) at Cornell University. A wide band-pass (1.47%) X-ray with a wavelength of 1.15 Å was shone on the samples with a grazing incidence angle of 0.15°. A Pilatus 200k area detector was placed at a distance of 195 mm from the samples. A 1.5 mm wide tantalum rod was used to block the intense scattering in the small-angle area. The exposure time was 1 s. High-resolution X-ray diffraction measurements were carried out at G2, CHESS at Cornell University. The thin films were aligned on a Kappa diffractometer to record the θ–2θ

scans. The wavelength of X-ray was 1.107 Å. An attenuator was used to allow ≈1/7 beam flux through and avoid saturation in the case of PBTTT sample at 200 °C annealing.

Device Fabrication and Characterization: All film preparation and characterization steps were carried out under inert atmosphere. Bottom-gate/top-contact devices were fabricated on heavily doped n^+-Si (100) wafers with 400 nm thick thermally grown SiO_2. The Si/SiO_2 substrates were treated with trichloro(octadecyl)silane to form a self-assembled monolayer. The polymers were dissolved in hot TCB (5 mg mL^{-1}) and spin cast at 2000 rpm from a hot solution for 60 s before being annealed at 200 °C for 30 min. Au (30 nm) source and drain electrodes were deposited onto the polymer film under vacuum through shadow masks. The channel width and length of the transistors are 1000 and 50 µm, respectively. Transistor characterization was carried out under nitrogen using a Keithley 4200 parameter analyzer. Mobility was extracted from the slope of $I_D^{1/2}$ versus V_G.

Supporting Information

Supporting Information is available from the Wiley Online Library or from the author. Additional data relating to the paper can be found at doi.org/10.6084/m9.figshare.1539547

Acknowledgements

This work was supported by the EPRSC through a Doctoral Training Grant and EP/K011987/1. CHESS is supported by the NSF & NIH/NIGMS via NSF award DMR-1332208. The authors thank Dr. Scott E. Watkins (CSIRO Melbourne) for the PESA measurements.

Received: July 9, 2015
Revised: August 26, 2015
Published online: October 19, 2015

[1] M. T. Dang, L. Hirsch, G. Wantz, *Adv. Mater.* **2011**, *23*, 3597.
[2] I. Osaka, R. D. McCullough, *Acc. Chem. Res.* **2008**, *41*, 1202.
[3] C. B. Nielsen, I. McCulloch, *Prog. Polym. Sci.* **2013**, *38*, 2053.
[4] R. Noriega, J. Rivnay, K. Vandewal, F. P. V Koch, N. Stingelin, P. Smith, M. F. Toney, A. Salleo, *Nat. Mater.* **2013**, *12*, 1038.
[5] S. Himmelberger, K. Vandewal, Z. Fei, M. Heeney, A. Salleo, *Macromolecules* **2014**, *47*, 7151.
[6] J. F. Chang, J. Clark, N. Zhao, H. Sirringhaus, D. W. Breiby, J. W. Andreasen, M. M. Nielsen, M. Giles, M. Heeney, I. McCulloch, *Phys. Rev. B* **2006**, *74*, 115318.
[7] R. J. Kline, M. D. McGehee, E. N. Kadnikova, J. Liu, J. M. J. Fréchet, *Adv. Mater.* **2003**, *15*, 1519.
[8] A. a. Virkar, S. Mannsfeld, Z. Bao, N. Stingelin, *Adv. Mater.* **2010**, *22*, 3857.
[9] H. N. Tsao, K. Müllen, *Chem. Soc. Rev.* **2010**, *39*, 2372.
[10] A. M. Hiszpanski, Y.-L. Loo, *Energy Environ. Sci.* **2014**, *7*, 592.
[11] X. Guo, M. Baumgarten, K. Müllen, *Prog. Polym. Sci.* **2013**, *38*, 1832.
[12] S. Holliday, J. E. Donaghey, I. McCulloch, *Chem. Mater.* **2014**, *26*, 647.
[13] I. McCulloch, M. Heeney, C. Bailey, K. Genevicius, I. Macdonald, M. Shkunov, D. Sparrowe, S. Tierney, R. Wagner, W. Zhang, M. L. Chabinyc, R. J. Kline, M. D. McGehee, M. F. Toney, *Nat. Mater.* **2006**, *5*, 328.
[14] B. H. Hamadani, D. J. Gundlach, I. McCulloch, M. Heeney, *Appl. Phys. Lett.* **2007**, *91*, 243512.
[15] M. L. Chabinyc, M. F. Toney, R. J. Kline, I. McCulloch, M. Heeney, *J. Am. Chem. Soc.* **2007**, *129*, 3226.
[16] J. R. Kline, D. M. DeLongchamp, D. A. Fischer, E. K. Lin, L. J. Richter, M. L. Chabinyc, M. F. Toney, M. Heeney, I. McCulloch, *Macromolecules* **2007**, *40*, 7960.
[17] Z. Fei, P. Pattanasattayavong, Y. Han, B. C. Schroeder, F. Yan, R. J. Kline, T. D. Anthopoulos, M. Heeney, *J. Am. Chem. Soc.* **2014**, *136*, 15154.
[18] J.-S. Wu, S.-W. Cheng, Y.-J. Cheng, C.-S. Hsu, *Chem. Soc. Rev.* **2015**, *44*, 1113.
[19] N. E. Jackson, B. M. Savoie, K. L. Kohlstedt, M. Olvera de la Cruz, G. C. Schatz, L. X. Chen, M. A. Ratner, *J. Am. Chem. Soc.* **2013**, *135*, 10475.
[20] X. Guo, J. Quinn, Z. Chen, H. Usta, Y. Zheng, Y. Xia, J. W. Hennek, R. P. Ortiz, T. J. Marks, A. Facchetti, *J. Am. Chem. Soc.* **2013**, *135*, 1986.
[21] H. G. Kim, B. Kang, H. Ko, J. Lee, J. Shin, K. Cho, *Chem. Mater.* **2015**, *27*, 829.
[22] T. Lei, X. Xia, J. Y. Wang, C. J. Liu, J. Pei, *J. Am. Chem. Soc.* **2014**, *136*, 2135.
[23] F. Babudri, G. M. Farinola, F. Naso, R. Ragni, *Chem. Commun.* **2007**, 1003.
[24] Z. Fei, P. Boufflet, S. Wood, J. Wade, J. Moriarty, E. Gann, E. L. Ratcliff, C. R. McNeill, H. Sirringhaus, J.-S. Kim, M. Heeney, *J. Am. Chem. Soc.* **2015**, *137*, 6866.
[25] J. W. Jo, J. W. Jung, H. W. Wang, P. Kim, T. P. Russell, W. H. Jo, *Chem. Mater.* **2014**, *26*, 4214.
[26] D. J. Crouch, P. J. Skabara, J. E. Lohr, J. J. W. McDouall, M. Heeney, I. McCulloch, D. Sparrowe, M. Shkunov, S. J. Coles, P. N. Horton, M. B. Hursthouse, *Chem. Mater.* **2005**, *17*, 6567.
[27] B.-G. Kim, E. J. Jeong, J. W. Chung, S. Seo, B. Koo, J. Kim, *Nat. Mater.* **2013**, *12*, 659.
[28] F. Gohier, P. Frère, J. Roncali, *J. Org. Chem.* **2013**, *78*, 1497.
[29] T. Umeda, S. Tokito, D. Kumaki, *J. Appl. Phys.* **2007**, *101*, 054517.
[30] I. McCulloch, M. Heeney, M. L. Chabinyc, D. DeLongchamp, R. J. Kline, M. Cölle, W. Duffy, D. Fischer, D. Gundlach, B. Hamadani, R. Hamilton, L. Richter, A. Salleo, M. Shkunov, D. Sparrowe, S. Tierney, W. Zhang, *Adv. Mater.* **2009**, *21*, 1091.
[31] M. L. Chabinyc, R. Lujan, F. Endicott, M. F. Toney, I. McCulloch, M. Heeney, *Appl. Phys. Lett.* **2007**, *90*, 233508.
[32] M. Zagórska, B. Krische, *Polymer* **1990**, *31*, 1379.
[33] S. Tierney, M. Heeney, L. McCulloch, *Synth. Met.* **2005**, *148*, 195.
[34] A. Gasperini, K. Sivula, *Macromolecules* **2013**, *46*, 9349.
[35] N. S. Colella, L. Zhang, T. McCarthy-Ward, S. C. B. Mannsfeld, H. H. Winter, M. Heeney, J. J. Watkins, A. L. Briseno, *Phys. Chem. Chem. Phys.* **2015**, DOI:10.1039/C4CP02944E.
[36] R. Hamilton, C. Bailey, W. Duffy, M. Heeney, M. Shkunov, D. Sparrowe, S. Tierney, I. Mcculloch, M. Chemicals, R. J. Kline, D. M. Delongchamp, M. Chabinyc, *Proc. SPIE* **2006**, *6336*, 633611.
[37] H. Wang, J. Liu, Y. Xu, Y. Han, *J. Phys. Chem. B* **2013**, *117*, 5996.
[38] J. S. Kim, J. H. Lee, J. H. Park, C. Shim, M. Sim, K. Cho, *Adv. Funct. Mater.* **2011**, *21*, 480.
[39] H. Xin, F. S. Kim, S. A. Jenekhe, *J. Am. Chem. Soc.* **2008**, *130*, 5424.
[40] S. Berson, R. De Bettignies, S. Bailly, S. Guillerez, *Adv. Funct. Mater.* **2007**, *17*, 1377.
[41] S. Samitsu, T. Shimomura, S. Heike, T. Hashizume, K. Ito, *Macromolecules* **2008**, *41*, 8000.
[42] D. M. DeLongchamp, R. J. Kline, Y. Jung, D. S. Germack, E. K. Lin, A. J. Moad, L. J. Richter, M. F. Toney, M. Heeney, I. McCulloch, *ACS Nano* **2009**, *3*, 780.
[43] D. M. DeLongchamp, R. J. Kline, Y. Jung, E. K. Lin, D. A. Fischer, D. J. Gundlach, S. K. Cotts, A. J. Moad, L. J. Richter, M. F. Toney, M. Heeney, I. McCulloch, *Macromolecules* **2008**, *41*, 5709.
[44] S.-Y. Jang, I.-B. Kim, J. Kim, D. Khim, E. Jung, B. Kang, B. Lim, Y.-A. Kim, Y. H. Jang, K. Cho, D. Kim, *Chem. Mater.* **2014**, *26*, 6907.
[45] T. Umeda, D. Kumaki, S. Tokito, *J. Appl. Phys.* **2009**, *105*, 024516.
[46] J. Soeda, H. Matsui, T. Okamoto, I. Osaka, K. Takimiya, J. Takeya, *Adv. Mater.* **2014**, *26*, 6430.
[47] H. Sirringhaus, *Adv. Mater.* **2014**, *26*, 1319.

[48] R. Schmidt, J. H. Oh, Y. Sen Sun, M. Deppisch, A. M. Krause, K. Radacki, H. Braunschweig, M. Könemann, P. Erk, Z. Bao, F. Würthner, *J. Am. Chem. Soc.* **2009**, *131*, 6215.
[49] H. E. Katz, A. J. Lovinger, J. Johnson, C. Kloc, T. Siegrist, W. Li, Y.-Y. Lin, A. Dodabalapur, *Nature* **2000**, *404*, 478.
[50] M. L. Chabinyc, F. Endicott, B. D. Vogt, D. M. DeLongchamp, E. K. Lin, Y. Wu, P. Liu, B. S. Ong, *Appl. Phys. Lett.* **2006**, *88*, 2004.
[51] M. L. Chabinyc, R. A. Street, J. E. Northrup, *Appl. Phys. Lett.* **2007**, *90*, 12.
[52] T. Lei, J.-H. Dou, Z.-J. Ma, C.-H. Yao, C.-J. Liu, J.-Y. Wang, J. Pei, *J. Am. Chem. Soc.* **2012**, *134*, 20025.
[53] T. Liu, A. Troisi, *Adv. Funct. Mater.* **2014**, *24*, 925.
[54] R. Noriega, J. Rivnay, K. Vandewal, F. P. V Koch, N. Stingelin, P. Smith, M. F. Toney, A. Salleo, *Nat. Mater.* **2013**, *12*, 1038.
[55] L. Biniek, N. Leclerc, T. Heiser, R. Bechara, M. Brinkmann, *Macromolecules* **2013**, *46*, 4014.
[56] N. C. Miller, E. Cho, M. J. N. Junk, R. Gysel, C. Risko, D. Kim, S. Sweetnam, C. E. Miller, L. J. Richter, R. J. Kline, M. Heeney, I. McCulloch, A. Amassian, D. Acevedo-Feliz, C. Knox, M. R. Hansen, D. Dudenko, B. F. Chmelka, M. F. Toney, J.-L. Brédas, M. D. McGehee, *Adv. Mater.* **2012**, *24*, 6071.
[57] K. Zhao, H. U. Khan, R. Li, Y. Su, A. Amassian, *Adv. Funct. Mater.* **2013**, *23*, 6024.
[58] D. T. Duong, V. Ho, Z. Shang, S. Mollinger, S. C. B. Mannsfeld, J. Dacuña, M. F. Toney, R. Segalman, A. Salleo, *Adv. Funct. Mater.* **2014**, *24*, 4515.
[59] M. J. Frisch, G. W. Trucks, H. B. Schlegel, G. E. Scuseria, M. A. Robb, J. R. Cheeseman, G. Scalmani, V. Barone, B. Mennucci, G. A. Petersson, H. Nakatsuji, M. Caricato, X. Li, H. P. Hratchian, A. F. Izmaylov, J. Bloino, G. Zheng, J. L. Sonnenberg, M. Hada, M. Ehara, K. Toyota, R. Fukuda, J. Hasegawa, M. Ishida, T. Nakajima, Y. Honda, O. Kitao, H. Nakai, T. Vreven, J. A. Montgomery Jr., J. E. Peralta, F. Ogliaro, M. J. Bearpark, J. Heyd, E. N. Brothers, K. N. Kudin, V. N. Staroverov, R. Kobayashi, J. Normand, K. Raghavachari, A. P. Rendell, J. C. Burant, S. S. Iyengar, J. Tomasi, M. Cossi, N. Rega, N. J. Millam, M. Klene, J. E. Knox, J. B. Cross, V. Bakken, C. Adamo, J. Jaramillo, R. Gomperts, R. E. Stratmann, O. Yazyev, A. J. Austin, R. Cammi, C. Pomelli, J. W. Ochterski, R. L. Martin, K. Morokuma, V. G. Zakrzewski, G. A. Voth, P. Salvador, J. J. Dannenberg, S. Dapprich, A. D. Daniels, Ö. Farkas, J. B. Foresman, J. V. Ortiz, J. Cioslowski, D. J. Fox, *Gaussian 09, Revision C.01*, Wallinford, CT, USA **2009**.